AIAA JOURNAL
Vol. 49, No. 6, June 2011

Interlaminar Shear Stresses Around Internal Elliptical Cylindrical Holes Weakening Edge-Loaded Cross-Ply Plates

Reaz A. Chaudhuri*
University of Utah, Salt Lake City, Utah 84112-0560
and
Paul Seide†
University of Southern California, Los Angeles, California 90089-2531

DOI: 10.2514/1.J050799

A semi-analytical postprocessing method, termed the equilibrium/compatibility method, is employed for computation of hitherto unavailable through-thickness variation of interlaminar shear stresses in the neighborhood of the bilayer interface circumferential reentrant corner line of an internal (part-through) elliptical cylindrical hole weakening an edge-loaded laminated composite plate. A C^0-type triangular composite plate element, based on the assumptions of transverse inextensibility and layerwise constant shear-angle theory, is used to first compute the in-plane stresses and layerwise through-thickness average interlaminar shear stresses, which serve as the starting point for computation of through-thickness distribution of interlaminar shear stresses in the vicinity of the bilayer interface circumferential reentrant corner line of the internal hole. The errors in the same stresses computed by the conventional equilibrium method are more severe in the presence of the bilayer interface circumferential reentrant corner line singularity arising out of the internal (part-through) elliptical cylindrical hole than their circular counterparts, and are, as before, found to violate the interfacial compatibility condition. The computed interlaminar shear stresses can vary from negative to positive through the thickness of a cross-ply plate in the neighborhood of this kind of stress singularity.

I. Introduction

INTERNAL (part-through) elliptical cylindrical holes are more realistic representations of internal cracklike flaws and damages that invariably occur during the manufacturing process, and propagate during service with catastrophic consequences [1–5]. The presence of internal part-through holes inside composite laminates is unavoidable in practice. A part of the internal material may be missing as a result of faulty manufacturing techniques. Although the issues concerning the weakening effects of through-thickness elliptical holes in laminated composite plates are well documented in the literature [6–8], the twin-problems of stress concentration and stress intensity in the vicinity of internal part-through holes weakening both homogeneous as well as laminated plates have till recently remained a virgin territory [1–5]. These interlaminar stresses in the neighborhood of such a hole in a stretched homogeneous isotropic as well as laminated anisotropic plate vary through the thickness, which brings three-dimensional effect even in a thin plate weakened by such an embedded (part-through) hole [1–5]. Finally, the effect of stress singularity in the neighborhood of the bilayer interface circumferential reentrant corner line of the internal hole weakening a laminated plate is also of serious concerns.

Majority of the finite element based postprocessing approaches employ equilibrium equations of three-dimensional elasticity theory, referred to here as the equilibrium method (EM) [9–14], the only exceptions being Chaudhuri and Seide [15], Chaudhuri [16] and Chaudhuri et al. [17]. The latter investigations have introduced a semi-analytical postprocessing method, termed the equilibrium/compatibility method, wherein both the equilibrium equations as well as interfacial compatibility conditions are satisfied in the pointwise sense. This latter approach has recently been employed for computation of hitherto unavailable through-thickness variation of transverse shear stresses in the vicinity of the circumferential reentrant corner lines of internal (part-through) circular and elliptical cylindrical holes weakening edge-loaded isotropic plates [18,19]. This also has recently been extended to the case of a cross-ply plate weakened by an internal (part-through) circular cylindrical hole [20]. A detailed review of the literature, however, reveals that the determination of interlaminar shear stresses in the vicinity of an internal (part-through) elliptical cylindrical hole weakening a laminated anisotropic plate, subjected to all-round tension, has still remained unaddressed in the literature. The primary objective of the present investigation is to fill this important gap. Of particular interest is the effect of internal hole geometry on the accuracy or lack thereof of interlaminar shear stresses, computed using the two approaches, i.e., the equilibrium method and the equilibrium/compatibility method.

In what follows, a curvilinear triangular element, based on the assumptions of transverse inextensibility and layerwise constant shear angle (LCST), is employed as a starting point to determine the through-thickness distribution of interlaminar or transverse shear stresses in the vicinity of an embedded (part-through) elliptical cylindrical hole, weakening a cross-ply plate, using a method that satisfies the equilibrium as well as interfacial compatibility in the pointwise sense. In this connection, it may be noted that the stress singularity, in the neighborhood of the bilayer interface circumferential reentrant corner line of the internal (part-through) hole, is that of a bimaterial wedge type singularity [21,22], of which the well-known free-edge stress singularity [23–26] is a special case.

II. Finite Element Formulation

An N-layer laminated composite triangular element (see figure 1 of [23]) with its bottom surface designated as the reference surface is employed here. The curvilinear triangular element is ideally suited for analysis of a laminated anisotropic plate weakened by a part-through hole of arbitrary geometry (e.g., elliptical, hyperbolic, etc.). The small deformation of such weakened plates [1–3] can be analyzed using a finite element formulated on the basis of assumptions of transverse inextensibility and layerwise constant shear

Received 27 July 2010; revision received 28 November 2010; accepted for publication 5 December 2010.

*Department of Materials Science and Engineering, 122 S. Central Campus Drive, Room 304; r.chaudhuri@utah.edu.

†Emeritus Professor, Department of Civil and Environmental Engineering, 3620 S. Vermont Avenue, KAP 210.

angle [27–29]. The special case of a moderately thick plate weakened by a through hole [30] can be analyzed by a finite element formulation based on the Mindlin hypothesis [31,32].

III. Determination of Interlaminar Shear Stresses Using the Equilibrium/Compatibility Method

Equations of equilibrium for a plate in curvilinear coordinates neglecting the body forces are given by

$$\tau^{lm}/_{l} = 0, \qquad m, l = 1(=\alpha), 2(=\beta), 3(=z) \tag{1}$$

where the covariant derivatives of contravariant components of stresses τ^{lm} are defined as

$$\tau^{lm}/_{l} = \tau^{lm}_{,l} + \Gamma^{m}_{lp}\tau^{lp} + \Gamma^{p}_{lp}\tau^{lm} \tag{2}$$

while the Euclidean–Christoffel symbol Γ^{m}_{lp} is defined as follows:

$$\Gamma^{m}_{lp} = \Gamma^{m}_{pl} = \frac{1}{2}g^{mn}(g_{np,l} + g_{ln,p} - g_{lp,n}) \tag{3}$$

with

$$g_{11} = \frac{1}{g^{11}}, \qquad g_{22} = \frac{1}{g^{22}}, \qquad g_{33} = 1, \qquad g_{mn} = g^{mn} = 0, \quad m \neq n \tag{4}$$

The relations (4) hold on account of selection of the orthogonal curvilinear coordinate system α, β, z, where α and β denote the directions of the coordinates of the plate reference (bottom) surface, while z denotes the direction of the normal to the reference surface. It is noteworthy that α, β, and z represent the local (or element) coordinates for the N-layer composite element.

A. General Flat Curvilinear Coordinates

The local or element coordinates are denoted by α, β, and z, while the corresponding global or plate coordinates are represented by x, y, z. Substitution of Eqs. (2–4) into Eq. (1), with $m = 1$ (or α), will lead to the first equation of equilibrium in terms of the physical components of the stresses:

$$\frac{\partial \tau^{(i)}_{\alpha z}(z)}{\partial z} = -\frac{1}{\bar{g}_\alpha \bar{g}_\beta}\left[\frac{1}{\bar{g}_\alpha}\frac{\partial}{\partial \beta}\{(\bar{g}_\alpha)^2 \tau^{(i)}_{\alpha\beta}(z)\} + \bar{g}_\beta \frac{\partial \sigma^{(i)}_{\alpha}(z)}{\partial \alpha} + \frac{\partial \bar{g}_\beta}{\partial \alpha}\{\sigma^{(i)}_{\alpha}(z) - \sigma^{(i)}_{\beta}(z)\}\right] \tag{5}$$

in which the curvilinear coordinates for the special case of elliptical geometry are given by $\alpha = n$, $\beta = s$, z [19,33]

$$\bar{g}_{\alpha} = \sqrt{g_{11}} = \bar{a}(\sinh^2 n + \sin^2 s)^{1/2} \tag{6a}$$

$$\bar{g}_{\beta} = \sqrt{g_{22}} = \bar{a}(\sinh^2 n + \sin^2 s)^{1/2} \tag{6b}$$

where

$$a = \bar{a}\cosh(n) \tag{6c}$$

$$c = \bar{a}\sinh(n) \tag{6d}$$

$$\bar{a} = \sqrt{(a^2 - c^2)} \tag{6e}$$

$$n = \tanh^{-1}(c/a) \tag{6f}$$

It may be noted here that n, s represent the elliptical coordinate system. **s** represents the tangential direction, while its magnitude is the angle the tangent makes with the y-axis (i.e., the normal makes with the x-axis) as shown in Fig. 1b. The second equation of equilibrium of elasticity can be obtained from Eq. (5) by replacing α by β and vice versa.

The left-hand sides of Eq. (A9) or Eq. (A10) can be obtained from the first equation of equilibrium, given by Eq. (5), as follows:

$$J^{(i+1)}_{\alpha} = -\frac{1}{\bar{g}_\alpha \bar{g}_\beta}\left\langle \frac{1}{\bar{g}_\alpha}\frac{\partial}{\partial \beta}[(\bar{g}_\alpha)^2\{\tau^{(i+1)}_{\alpha\beta}(0) - \tau^{(i)}_{\alpha\beta}(t_i)\}] + \bar{g}_\beta \frac{\partial}{\partial \alpha}\{\sigma^{(i+1)}_{\alpha}(0) - \sigma^{(i)}_{\alpha}(t_i)\} + \frac{\partial \bar{g}_\beta}{\partial \alpha}\{\sigma^{(i+1)}_{\alpha}(0) - \sigma^{(i)}_{\alpha}(t_i) - \sigma^{(i+1)}_{\beta}(0) + \sigma^{(i)}_{\beta}(t_i)\}\right\rangle \tag{7}$$

B. Fixed Natural Coordinates Basis Vectors Approximation

The natural coordinate basis vectors, defined by Park and Stanley [34] as

$$\mathbf{a}_r \approx \mathbf{g}_r/\sqrt{g_{rr}}, \qquad r = 1, 2, (\text{no sum on } r) \tag{8}$$

where

$$\mathbf{g}_r = \frac{\partial x^m}{\partial \theta^r}\mathbf{i}_m, \qquad m, r = 1, 2, 3 \tag{9}$$

can be assumed to be fixed, when subjected to differentiation with respect to α and β. This implies that for sufficiently small elements, which is reasonable to expect at the time of convergence

$$\mathbf{g}_r \approx \sqrt{g_{rr}}\mathbf{a}_r \approx \sqrt{g_{rr}}\mathbf{i}_r, \qquad r = 1, 2, 3(\text{no sum on } r) \tag{10}$$

This approximation helps simplify Eq. (5) and consequently, Eq. (7) in the following manner. Computation of the various derivatives of the surface-parallel components of stresses with respect to α and β, which appear in Eq. (7) would involve additional computations, and also a slower rate of convergence, when obtained using an assumed displacement finite element method (FEM). The computation of these derivatives is avoided by integration of both sides of Eq. (5) over the surface area of a triangular element, and then application of the divergence (Green–Gauss) theorem [15,16]. This procedure, in conjunction with the approximation given by Eq. (10), simplifies, e.g., the first equation of equilibrium, given by Eq. (5), as follows:

$$\iint_{S_j} \frac{\partial \tau^{(i)}_{\alpha z}}{\partial z}\,\mathrm{d}S = -\iint_{S_j} \sigma^{(i)}_{\alpha m, m}(z)\,\mathrm{d}S = -\sum_{k=1}^{3}\int_{\bar{\Gamma}^{(k)}_j} \sigma^{(i)}_{\alpha m}(z)\bar{n}^{(k)}_m\,\mathrm{d}\Gamma, \quad m = 1(=\alpha), 2(=\beta) \tag{11}$$

in which $\bar{s}_j$ and $\bar{\Gamma}_j$ are the area and perimeter, respectively, of the jth triangular element, while $\bar{n}^{(k)}_m$ at a point on the kth side of the curved triangle can be obtained in a manner described in Appendix of Chaudhuri [16]. Equation (7) can also be simplified in a similar manner.

C. Cartesian-Like Local Riemann Coordinates Approximation

Every Riemann space admits local Riemann coordinates for any given origin, where all the Chistoffel symbols vanish [11,16,35]. The Riemann coordinates with origin in the present context may be defined as

$$x = \int_0^x \bar{g}_\alpha\,\mathrm{d}\alpha \tag{12a}$$

$$y = \int_0^y \bar{g}_\beta\,\mathrm{d}\beta \tag{12b}$$

These Riemann coordinates may be thought to behave like rectangular Cartesian coordinates in the vicinity of the local or element origin, because every Riemann space also is locally Euclidean (i.e., admits rectangular Cartesian coordinates), which implies that every

sufficiently small (infinitesimally small in the limit) portion of a Riemann space is Euclidean. Since for quadratic shape functions $\sigma^{(i)}_{xm,m}$ $(m = x, y)$ is constant with respect to x, y, under the Cartesian-like Riemann coordinates (CLRC) approximation, integrating Eq. (7) over the area of the element and dividing by the same will not alter anything. This step yields $\frac{\partial \tau^{(i)}_{\alpha z}(z)}{\partial z}$ in the ith layer as follows:

$$\frac{\partial \tau^{(i)}_{\alpha z}}{\partial z} = \frac{1}{S_j}\iint_{S_j} \frac{\partial \tau^{(i)}_{\alpha z}}{\partial z}\,\mathrm{d}S \approx \frac{1}{S_j}\iint_{S_j} \frac{\partial \tau^{(i)}_{xz}}{\partial z}\,\mathrm{d}S$$
$$= -\frac{1}{S_j}\left[\iint_{S_j} \sigma^{(i)}_{xm,m}(z)\,\mathrm{d}S\right] = -\frac{1}{S_j}\left[\sum_{k=1}^{3}\int_{\Gamma^{(k)}_j} \sigma^{(i)}_{xm}(z) n^{(k)}_m\,\mathrm{d}\Gamma\right] \quad (13)$$

where $n^{(k)}_m$ for $m = 1$ $(=x)$, 2 $(=y)$ and $\Gamma^{(k)}_j$ for $k = 1, \ldots, 3$ for the jth triangular element are given by equations (A14) and (A15), respectively, of [20] (see also figure eight of [20]). As the in-plane stresses, $\sigma^{(i)}_\alpha$, etc., are linear functions of x and y, one Gauss point is sufficient for exact integration on each side of the triangle. Besides, the in-plane stresses at the midpoints of the sides are exceptionally accurate (Barlow points). This step yields the jump in $\frac{\partial \tau_{\alpha z}(z)}{\partial z}$ at the $(i+1)$th interface as given below:

$$J^{(i+1)}_\alpha = \frac{\partial \tau^{(i+1)}_{\alpha z}(0)}{\partial z} - \frac{\partial \tau^{(i)}_{\alpha z}(t_i)}{\partial z} \approx \frac{\partial \tau^{(i+1)}_{xz}(0)}{\partial z} - \frac{\partial \tau^{(i)}_{xz}(t_i)}{\partial z}$$
$$\approx -\frac{1}{S_j}[\{\sigma^{(i+1)}_x(0)|_{\text{Node }2} y_1 - \tau^{(i+1)}_{xy}(0)|_{\text{Node }2} x_1$$
$$+ \sigma^{(i+1)}_x(0)|_{\text{Node }4}(y_2 - y_1) - \tau^{(i+1)}_{xy}(0)|_{\text{Node }4}(x_2 - x_1)$$
$$- \sigma^{(i+1)}_x(0)|_{\text{Node }6} y_2 + \tau^{(i+1)}_{xy}(0)|_{\text{Node }6} x_2\} - \{\sigma^{(i)}_x(t_i)|_{\text{Node }2} y_1$$
$$- \tau^{(i)}_{xy}(t_i)_{\text{Node }2} x_1 + \sigma^{(i)}_x(t_i)|_{\text{Node }4}(y_2 - y_1) - \tau^{(i)}_{xy}(t_i)|_{\text{Node }4}(x_2$$
$$- x_1) - \sigma^{(i)}_x(t_i)|_{\text{Node }6} y_2 + \tau^{(i)}_{xy}(t_i)|_{\text{Node }6} x_2\}],$$
$$\text{for } i = 1, \ldots, N-1 \quad (14)$$

where $J^{(i+1)}_\alpha$, $i = 1, \ldots, N-1$, is given by Equation (7).

Finally, Eqs. (A6a), (A6b), and (A8) and the combination of Eqs. (A10) and (14) determine the $3N$ unknown parameters required for describing the $\tau_{\alpha z}(z) \approx \tau_{xz}(z)$ distribution through the thickness of the N-layer laminated anisotropic plate under investigation. Following an identical procedure and using the second equation of equilibrium, $\tau_{\beta z}(z) \approx \tau_{yz}(z)$ distribution through the laminate thickness can be determined. The centroid of the quadratic triangular element is the point of exceptional accuracy for the interlaminar shear stresses [15].

IV. Numerical Results and Discussions

The cross-ply plate, shown in Fig. 1, has three distinct layers $(90°/0°/90°)$, the middle layer having the same thickness as that of the internal part-through elliptical cylindrical hole. $\bar{\theta}_i = 0°$ denotes fibers in the ith layer being laid up parallel to x-axis. A and A' denote bottom and top corner points, the loci of which represent circumferential bilayer interface reentrant corner lines of an internal part-through elliptical cylindrical hole weakening an edge-loaded rectangular cross-ply plate in Fig. 1a. The following geometric parameters are selected: $L = 50.8$ cm (20 in.), $b = 35.56$ cm (14 in.), $t = 0.762$ cm (0.3 in.), $a = 5.04$ cm (2 in.), $c = 2.54$ cm (1 in.), $h = 0.504$ cm (0.2 in.). The orthotropic lamina elastic properties are as follows: $E_{11} = 275.8$ GPa (40 Msi), $E_{22} = 6.895$ GPa (1 Msi), $G_{12} = G_{13} = G_{23} = 3.4475$ GPa (0.5 Msi), $\nu_{12} = \nu_{13} = 0.25$, $\nu_{23} = 0.25$. Here E_{11} and E_{22} represent Young's moduli in the direction of the fibers and transverse to the fibers, respectively, while G_{12} denotes the in-plane shear modulus. G_{13} and G_{23} represent the transverse shear moduli in the planes parallel and normal to the fiber direction, respectively. ν_{12} denotes the major Poisson's ratio in the plane of the lamina, while ν_{13} and ν_{23} represent major Poisson's ratios in the transverse planes parallel and normal to the fiber direction, respectively. The plate is subjected to all-round tension, $q = 689.5$ kPa (100 psi). The finite element model is the same as figure 4 of Chaudhuri [3]. The interlaminar shear stresses, computed by the present equilibrium/compatibility method, have been obtained by using the reduced integration.

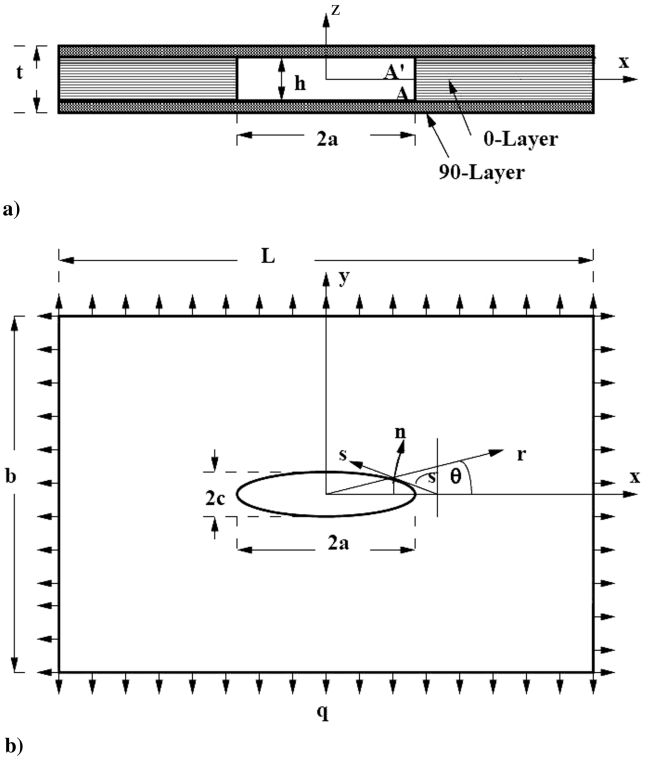

Fig. 1 Rectangular cross-ply plate weakened by an internal part-through elliptical cylindrical hole under all-round tension.

Figures 2 and 3 present variation of the midsurface normalized interlaminar (transverse) shear stresses, $\tau^*_{nz} = 100\tau^{(2)}_{nz}(t_2/2)/q$ and $\tau^*_{sz} = 100\tau^{(2)}_{sz}(t_2/2)/q$, computed at the centroids of the triangular elements adjacent to the boundary of the internal part-through elliptical hole (see also Table 1), with respect to s. The present solutions feature a nearly constant interlaminar shear stress variation in regards to the angular position, while their equilibrium counterparts show a radically different trend, primarily as a result of oscillations. As has been observed in the case of an internal part-through circular [18] and elliptical [19] hole weakening a homogeneous isotropic plate or an internal part-through circular hole weakening a cross-ply plate [20], the results for interlaminar or transverse shear stresses, computed using the equilibrium method, are in serious errors and even more so than their circular counterparts. In comparison to their counterparts for the homogeneous isotropic

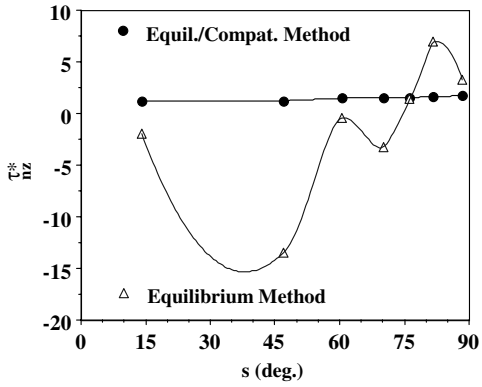

Fig. 2 Variation of the normalized transverse shear stresses a) τ_{nz} and b) τ_{sz}, around the circumference of an internal part-through elliptical cylindrical hole (see also Table 1).

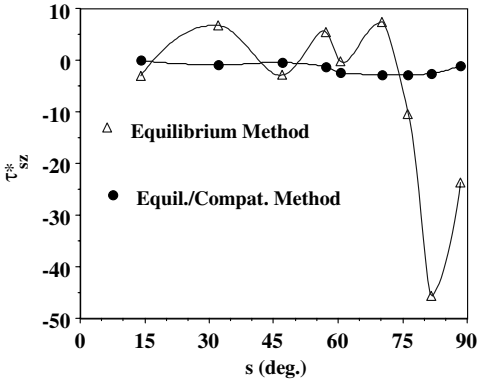

Fig. 3 Through-thickness variation of normalized transverse shear stress, $100\tau_{nz}/q$, in the vicinity of an internal part-through elliptical cylindrical hole ($x = 1.5103$ cm (0.5946 in.), $y = 2.5842$ cm (1.0174 in.), $s = 81.6875°$).

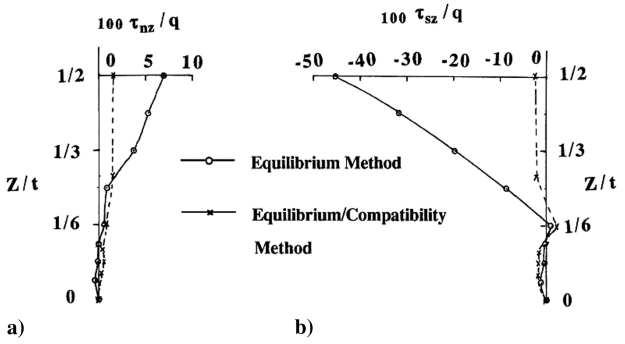

Fig. 4 Through-thickness variation of normalized transverse shear stress, $100\tau_{sz}/q$, in the vicinity of an internal part-through elliptical cylindrical hole ($x = 1.5103$ cm (0.5946 in.), $y = 2.5842$ cm (1.0174 in.), $s = 81.6875°$).

case [19], the interlaminar (or transverse) shear stresses, computed using the equilibrium method, are characterized by much larger oscillations as compared with those computed using the present equilibrium/compatibility method in more or less the entire range of s. Figure 2 shows a significantly larger error in the interlaminar shear stress, τ^*_{nz}, vs s curve, in the neighborhood of the bilayer interface circumferential reentrant corner line of the internal part-through elliptical hole, in the range, $0° < s < 60°$, and relatively speaking, smaller error in the range, $70° < s < 90°$, as compared with its circular counterpart (see figure 4 of [20]). Figure 3 displays more severe oscillations in τ^*_{sz} vs s curve, computed using the equilibrium method, as compared with its circular counterpart (see figure 5 of [20]), although the latter produces larger error in θ close to 90°. These errors are also influenced by the interactions of the free-edge stress singularities at the boundaries, $x = L/2$ and $y = b/2$, with that resulting from the presence of the internal elliptical cylindrical hole. It may be recalled in this connection that for a cross-ply laminate compromised by the presence of an embedded part-through elliptical hole in the middle layer, in addition to the near-field stress singularity at the circumferential line of intersection of the part-though hole with the material of the middle layer in the form of a circumferential bilayer interface reentrant corner, there is a far-field free-edge stress singularity at the bilayer interface at each of the plate boundaries, $x = L/2$, and $y = b/2$. These two types (i.e., far-field and near-field) of stress singularities interact rather strongly so that the effect of the internal part-through hole never dies down at the plate boundary [2,3], and St. Venant's principle does not hold in this situation [21]. This is unlike what has been shown for the homogeneous isotropic plate weakened by an identical part-through hole [1,3].

Figures 4a and 4b show variation of $\tau^{(i)}_{nz}(z)$ and $\tau^{(i)}_{sz}(z)$ through the thickness at $x = 1.5103$ cm (0.5946 in.), $y = 2.5842$ cm (1.0174 in.), $s = 81.6875°$. As has been stated earlier, and also can be seen from Figs. 4a and 4b the transverse shear stress distribution through the thickness computed by the equilibrium method is in serious error. Since the layer-material is homogeneous, $\tau^{(i)}_{nz}$ vs z curve cannot have a "corner" within a layer, because that would imply jumps (or discontinuities) in the stresses, $\sigma^{(i)}_n(z)$ and $\tau^{(i)}_{ns}(z)$, which, in turn, would imply jumps in strains, $\varepsilon^{(i)}_n(z)$ and $\gamma^{(i)}_{ns}(z)$, and consequently discontinuities in in-plane displacements at that particular z, i.e., the compatibility conditions are violated [18–20]. The apparent reason behind this lack of accuracy in the result computed by the equilibrium method is that there is only one integration constant, which cannot make the computed transverse shear stress vanish on both the bottom and top surfaces of plate, unless symmetry with respect to the middle surface is invoked [18–20]. The error in $\frac{\partial \sigma^{(i)}_x(z)}{\partial x} + \frac{\partial \tau^{(i)}_{xy}(z)}{\partial y}$ computed by the finite element method is "body force" like (constant through thickness in uniform stretching problems), and is of the order of $\frac{\partial \tau^{(i)}_{xz}(z)}{\partial z}$. When $\tau^{(i)}_{xz}(z)$ is computed by the equilibrium method by integrating the first equation of equilibrium through thickness, this error shows up as a straight line. In the case of a symmetrically (with respect to the middle surface) placed internal part-through elliptical cylindrical hole weakening a symmetrically laminated cross-ply plate subjected to uniform stretching, if $\tau^{(i)}_{xz}(z)$ through half the thickness is computed by using the equilibrium method, and the same through the other half is obtained by using symmetry, this would result in the formation of a corner in the curve at the midsurface, which cannot be acceptable because of the violation of the compatibility condition at the midsurface of the plate in the immediate neighborhood of the bilayer interface circumferential reentrant corner line.

It is worthwhile to note from figure 10 of Chaudhuri [3] that $\sigma^{(i)}_x(z)$ at the bilayer interface (circumferential reentrant corner line) experiences a jump at the circumference of the internal part-through elliptical cylindrical hole, and that the maximum stress occurs at this corner. The slope of the above curve (i.e., $\sigma^{(i)}_{x,x}(z)$) at the bilayer interface circumferential reentrant corner is approximately $\tan(\pi/2) = \infty$, which, when substituted into the equilibrium equations, will yield singular transverse stresses, $\tau^{(i)}_{xz}(z)$ and $\sigma^{(i)}_z(z)$, in that neighborhood. Figure 7 of [20] displays the state of stress in a 270° bimaterial wedge shaped plane section normal to the bilayer interface

Table 1 Variation of transverse shear stresses at the midsurface around the circumference of a part-through elliptical hole in a rectangular cross-ply plate

Location			$\frac{100\tau^2_{nz}(t_{2/2})}{q}$		$\frac{100\tau^2_{sz}(t_{2/2})}{q}$	
$\bar{x}$	$\bar{y}$	s, deg	Equilibrium method	Equilibrium/compatibility method	Equilibrium method	Equilibrium/compatibility method
2.045	0.127	13.980	−2.002	1.147	−3.080	−0.069
1.839	0.481	46.924	−13.430	1.235	−2.904	−0.430
1.650	0.638	57.120	−5.196	0.727	5.415	−1.375
1.501	0.727	60.422	−0.426	1.478	−0.275	−2.388
1.233	0.850	70.070	−3.235	1.559	7.395	−2.844
0.928	0.948	76.253	1.429	1.537	−10.391	−2.893
0.595	1.017	81.688	6.907	1.630	−45.665	−2.564
0.116	1.062	88.438	3.221	1.715	−23.717	−1.034

circumferential line of intersection of the boundary wall of the internal (circular/elliptical) part-through hole with its ceiling or floor (locus of point A or A' in Fig. 1). The local coordinate system in that figure is composed of R, which denotes the radial direction from a point located on the circumferential line of intersection of the bottom interior surface of the plate and the hole, ϕ, which denotes the angular direction measured counterclockwise from the hole surface, and s, which is positive counterclockwise (looking from top) along the circumferential line of intersection of the interior surface of the plate and the hole surface. The stresses,$\sigma_R^{(i)}$, $\sigma_\phi^{(i)}$, $\tau_{R\phi}^{(i)}$, and $\sigma_s^{(i)}$, are singular in the vicinity of the bilayer interface circumferential reentrant corner line of the internal part-through hole [5,26]. This translates into rendering $\sigma_n^{(i)}$, $\tau_{nz}^{(i)}$, $\sigma_z^{(i)}$, and $\sigma_s^{(i)}$ singular in that neighborhood. The stress field varies as $R^{-\lambda}$, $0 < \lambda < 1$, in the vicinity of the bilayer interface circumferential corner line of the part-through hole. In the presence of a stress singularity of this kind, the stress gradients are also significantly large, which combined with the constant (through the thickness) term causes the above-mentioned "body force' like error upon integration with respect to z, when the equilibrium method is used. This implies that the artificial corner (see Figs. 4a and 4b) will appear whenever in-plane stress gradients do not vanish at the midsurface of the plate, and consequently the equilibrium method will fail to deliver accurate results for the interlaminar shear stresses.

The above-mentioned corner and the associated "body force" like error can be eliminated by using the present method as can be seen from Figs. 4a and 4b because of its satisfaction of the bilayer interface compatibility condition, given by Eq. (7) or Eq. (14) in combination with Eq. (A10), in the form of the condition (iv) of Sec. III. In this connection, it may be remarked that the accuracy (or lack thereof) of the equilibrium method is a good indicator of the accuracy of the computed intralaminar (in-plane) stresses (strictly speaking stress gradients), since this method depends on equilibrium of these stresses. This is in line with the fact that the computed in-plane stresses including $\sigma_s^{(i)}$ computed at the edge of the hole at or near $s \sim 90°$ may be in some error. As has been discussed earlier [18–20], the subparametric version of the assumed quadratic displacement triangular element cannot accurately predict the stresses in the elements located inside the "boundary-layer" zone.

A comparison of the computed through-thickness distribution of the interlaminar shear stress, $\tau_{nz}^{(i)}$, in the vicinity of an internal part-through elliptical cylindrical hole, shown in Fig. 4a, with its counterpart for a homogeneous plate, shown in figure 4 of Chaudhuri [19], reveals that the present interlaminar shear stress, $\tau_{nz}^{(i)}$, can vary from negative to positive through the thickness of a cross-ply plate in the neighborhood of the above-mentioned kind of stress singularity, while its homogeneous isotropic counterpart is always positive, other factors remaining unaltered. Furthermore, the interlaminar shear stress, $\tau_{nz}^{(i)}$, is, in the present case, much smaller in magnitude than its counterpart for a homogeneous isotropic plate.

V. Conclusions

The present investigation deals with the important issue of simultaneously satisfying the pointwise equilibrium and compatibility conditions of elasticity theory by the stresses computed using the conventional FEM in the vicinity of a stress singularity. It reaffirms, to a rather more extreme degree, the conclusion reached earlier in the case of its homogeneous counterpart [19] in regards to the accuracy (or lack thereof) of the stresses computed using the conventional (assumed displacement potential energy based) finite element analysis and computed FEM-based postprocessing analysis results for interlaminar shear stresses in the vicinity of a stress singularity, such as the bilayer interface circumferential corner line of an internal elliptical cylindrical hole. Equation (7) or Eq. (14), in combination with Eq. (A10), constitutes the required layer-interface compatibility equation, when a weak or integral form of solution (in Sobolev space, H^1) is sought with convergence in the L_2 norm [18–20]. This equation is the counterpart of the compatibility (differential) equation (see the last part of equation 4, p. 101, Fung [36]) when strong or differential form of solution is sought with convergence in the sup norm. The following important conclusions are drawn from the numerical results of the present finite element based postprocessing analysis:

1) The present solutions features a nearly constant interlaminar shear stress variation in regards to the angular position, while their equilibrium counterparts show a different trend, primarily as a result oscillations discussed below in item 3.

2) The transverse shear stress $\tau_{nz}^{(i)}$ computed using the conventional equilibrium method is in serious error in the presence of the stress singularity at the circumferential reentrant corner line of an internal part-through elliptical cylindrical hole. This is because $\tau_{nz}^{(i)}$ is singular. This error is "body force" like, and is due to the violation of the compatibility equation in the presence of stress singularity.

3) In comparison with their counterparts for the homogeneous isotropic case, the interlaminar (or transverse) shear stresses computed using the equilibrium method are characterized by much larger oscillations (errors) as compared with those computed using the present equilibrium/compatibility method in more or less the entire range of s.

4) The errors in the interlaminar shear stresses (computed using the equilibrium method) vs s curves, in the neighborhood of the bilayer interface circumferential reentrant corner line of the internal part-through elliptical cylindrical hole are characterized by even larger oscillations than their circular counterparts.

5) As in the case of its circular counterpart, two types of stress singularities (i.e., near-field and far-field) interact so that the effect of the internal part-through elliptical hole never dies down at the plate boundary, and St. Venant's principle does not hold in this situation. This is unlike what has been shown for the homogeneous isotropic plate weakened by an otherwise identical part-through hole.

6) The above error can be eliminated by using the present method because of its satisfaction of layer-interface compatibility condition in the vicinity of the circumferential reentrant corner line singularity arising out of the internal part-through hole.

7) A comparison of the computed through-thickness distribution of the interlaminar shear stress, $\tau_{nz}^{(i)}$, in the vicinity of an internal part-through elliptical cylindrical hole with its counterpart for a homogeneous plate reveals that the present interlaminar shear stress can vary from negative to positive through the thickness of a cross-ply plate in the neighborhood of the above-mentioned kind of stress singularity, while its homogeneous isotropic counterpart is always positive, other factors remaining unaltered. Furthermore, the interlaminar shear stress, $\tau_{nz}^{(i)}$, is, in the present case, much smaller in magnitude than its counterpart for a homogeneous isotropic plate.

Appendix

Once the nodal displacements are computed using the finite element method, the layer-element stresses can be obtained using the following relation [15,16]:

$$\{\sigma^{(i)}(z)\}^T = [C^{(i)}][A^{(i)}(z)][B_j^{(i)}]\{d_j^{(i)}\} \tag{A1}$$

where α and β are general curvilinear coordinates in the plane of the plate, z is the transverse coordinate local to the ith layer, and is measured from its bottom surface, and

$$\{\sigma^{(i)}(z)\}^T = \{\,\sigma_\alpha^{(i)}(z),\quad \sigma_\beta^{(i)}(z),\quad \tau_{\alpha\beta}^{(i)}(z),\quad \bar{\tau}_{\alpha z}^{(i)},\quad \bar{\tau}_{\beta z}^{(i)}\,\} \tag{A2}$$

while $[A^{(i)}(z)]$, $[C^{(i)}]$ and $\{d_j^{(i)}\}$ are as given by Eqs. (A1), (A3), and (A7), respectively, in the appendix of [20]. $[B_j^{(i)}]$ is given by Eq. (A8) of [20], except the following:

$$[R_k] = \begin{bmatrix} \frac{\phi_{k,\alpha}}{g_\alpha} & \frac{g_{\alpha,\beta}\phi_k}{g_\alpha g_\beta} \\ \frac{g_{\beta,\alpha}\phi_k}{g_\alpha g_\beta} & \frac{\phi_{k,\beta}}{g_\beta} \\ -\frac{g_{\beta,\alpha}\phi_k}{g_\alpha g_\beta} + \frac{\phi_{k,\beta}}{g_\beta} & -\frac{g_{\alpha,\beta}\phi_k}{g_\alpha g_\beta} + \frac{\phi_{k,\alpha}}{g_\alpha} \end{bmatrix} \tag{A3a}$$

$$[T_k]^T = \begin{bmatrix} \frac{\phi_{k,\alpha}}{g_\alpha} & \frac{\phi_{k,\beta}}{g_\beta} \end{bmatrix} \tag{A3b}$$

in which ϕ_k, $k = 1, \ldots, 6$, represents the shape function [3].

The assumption of LCST implies parabolic variation of interlaminar (transverse) shear strains and stresses through the thickness of a layer. This implies, for example, that $\tau_{\alpha z}^{(i)}(z)$ is of the form [15,16]:

$$\tau_{\alpha z}^{(i)}(z) = N_1(z)\bar{f}_1^{(i)} + N_2(z)\bar{f}_2^{(i)} + N_3(z)\bar{f}_3^{(i)} \tag{A4}$$

where $\bar{f}_1^{(i)}$, $\bar{f}_2^{(i)}$ and $\bar{f}_3^{(i)}$ represent $\tau_{\alpha z}^{(i)}(z)$ at the bottom, middle and top surface, respectively, of the ith layer. $N_1(z)$, $N_2(z)$ and $N_3(z)$ are one-dimensional quadratic shape functions, defined by

$$\begin{aligned} N_1(z) &= 1 - \frac{3z}{t_i} + \frac{2z^2}{t_i^2}, \qquad N_2(z) = \frac{4z}{t_i} - \frac{4z^2}{t_i^2}, \\ N_3(z) &= -\frac{z}{t_i} + \frac{2z^2}{t_i^2} \end{aligned} \tag{A5}$$

$\tau_{\alpha z}(z)$ distribution through the thickness of an N-layer laminate, therefore, requires $3N$ unknown parameters, which, in turn, ask for $3N$ equations. The present equilibrium/ compatibility method supplies these equations, by 1) forcing $\tau_{\alpha z}$ to vanish on the top and bottom surfaces of the laminate (2 equations), 2) satisfying continuity of $\tau_{\alpha z}$ at each layer-interface ($N - 1$ equations), 3) identifying $\bar{\tau}_{\alpha z}^{(i)}$, as computed by Eqs. (A1) and (A2) above, as the through-the-layer-thickness average of $\tau_{\alpha z}^{(i)}(z)$ (N equations), and 4) computing jump in $\tau_{\alpha z,z}$ at each interface using the first equation of equilibrium in terms of stresses ($N - 1$ equations) [15,16].

Conditions 1 and 2 above imply

$$\bar{f}_1^{(1)} = \bar{f}_3^{(N)} = 0 \tag{A6a}$$

$$\bar{f}_1^{(i)} = \bar{f}_3^{(i-1)}, \qquad i = 2, \ldots, N \tag{A6b}$$

The condition (3) yields

$$\begin{aligned} &\frac{1}{t_i}\int_0^{t_i} \tau_{\alpha z}^{(i)}(z)\,\mathrm{d}z \\ &\quad = [0, \quad 0, \quad 0, \quad 0, \quad 0, \quad 0, \quad c_{44}^{(i)}, \quad c_{45}^{(i)}][B_j^{(i)}]\{d_j^{(i)}\}, \\ &\quad \text{for } i = 1, \ldots, N \end{aligned} \tag{A7}$$

which, with the help of Eqs. (A4–A7), become

$$\begin{aligned} &\left(\frac{1}{6}\bar{f}_1^{(i)} + \frac{2}{3}\bar{f}_2^{(i)} + \frac{1}{6}\bar{f}_3^{(i)}\right) \\ &\quad = [0, \quad 0, \quad 0, \quad 0, \quad 0, \quad 0, \quad c_{44}^{(i)}, \quad c_{45}^{(i)}][B_j^{(i)}]\{d_j^{(i)}\}, \\ &\quad \text{for } i = 2, \ldots, N-1 \end{aligned} \tag{A8a}$$

$$\begin{aligned} &\left(\frac{2}{3}\bar{f}_2^{(1)} + \frac{1}{6}\bar{f}_3^{(1)}\right) \\ &\quad = [0, \quad 0, \quad 0, \quad 0, \quad 0, \quad 0, \quad c_{44}^{(1)}, \quad c_{45}^{(1)}][B_j^{(1)}]\{d_j^{(1)}\} \end{aligned} \tag{A8b}$$

$$\begin{aligned} &\left(\frac{1}{6}\bar{f}_3^{(N-1)} + \frac{2}{3}\bar{f}_2^{(N)}\right) \\ &\quad = [0, \quad 0, \quad 0, \quad 0, \quad 0, \quad 0, \quad c_{44}^{(N)}, \quad c_{45}^{(N)}][B_j^{(N)}]d_j^{(N)} \end{aligned} \tag{A8c}$$

The left and right sides of the remaining $N - 1$ equations are given by the condition 4 above, and are obtained by using Eqs. (A4) and (A5) and the first equation of equilibrium, respectively.

The jump at the $(i + 1)$th interface as computed using Eq. (A4), is given as follows:

$$\begin{aligned} J_\alpha^{(i+1)} &= \frac{\partial \tau_{\alpha z}^{(i+1)}(0)}{\partial z} - \frac{\partial \tau_{\alpha z}^{(i)}(t_i)}{\partial z} = \left[\frac{\partial N_1(z)}{\partial z}\bar{f}_3^{(i)} + \frac{\partial N_2(z)}{\partial z}\bar{f}_2^{(i+1)}\right. \\ &\quad \left. + \frac{\partial N_3(z)}{\partial z}\bar{f}_3^{(i+1)}\right]_{z=0} - \left[\frac{\partial N_1(z)}{\partial z}\bar{f}_3^{(i-1)} + \frac{\partial N_2(z)}{\partial z}\bar{f}_2^{(i)}\right. \\ &\quad \left. + \frac{\partial N_3(z)}{\partial z}\bar{f}_3^{(i)}\right]_{z=t_i} \end{aligned} \tag{A9}$$

which, with the help of Eq. (A5), becomes

$$\begin{aligned} J_\alpha^{(i+1)} &= -\frac{1}{t_i}\bar{f}_3^{(i-1)} + \frac{4}{t_i}\bar{f}_2^{(i)} - 3\left(\frac{1}{t_i} + \frac{1}{t_{i+1}}\right)\bar{f}_3^{(i)} \\ &\quad + \frac{4}{t_{i+1}}\bar{f}_2^{(i+1)} - \frac{1}{t_{i+1}}\bar{f}_3^{(i+1)}, \quad \text{for } i = 2, \ldots, N-2 \end{aligned} \tag{A10a}$$

$$J_\alpha^{(2)} = \frac{4}{t_1}\bar{f}_2^{(1)} - 3\left(\frac{1}{t_1} + \frac{1}{t_2}\right)\bar{f}_3^{(1)} + \frac{4}{t_2}\bar{f}_2^{(2)} - \frac{1}{t_2}\bar{f}_3^{(2)} = 0 \tag{A10b}$$

$$\begin{aligned} J_\alpha^{(N)} &= -\frac{1}{t_{N-1}}\bar{f}_3^{(N-2)} + \frac{4}{t_{N-1}}\bar{f}_2^{(N-1)} - 3\left(\frac{1}{t_{N-1}} + \frac{1}{t_N}\right)\bar{f}_3^{(N-1)} \\ &\quad - \frac{4}{t_N}\bar{f}_2^{(N)} \end{aligned} \tag{A10c}$$

Acknowledgment

The authors gratefully acknowledge the support of NASA Langley Research Center, Hampton, VA, under the grant no. NSG 1401.

References

[1] Chaudhuri, R. A., and Seide, P., "Triangular Element for Analysis of a Stretched Plate Weakened by a Part-Through Hole," *Computers and Structures*, Vol. 24, No. 1, 1986, pp. 97–105. doi:10.1016/0045-7949(86)90338-X

[2] Chaudhuri, R. A., "Stress Concentration around a Part-Through Hole Weakening a Laminated Plate," *Computers and Structures*, Vol. 27, No. 5, 1987, pp. 601–609. doi:10.1016/0045-7949(87)90075-7

[3] Chaudhuri, R. A., "Weakening Effects of Internal Part-through Elliptic Holes on Homogeneous and Laminated Composite Plates," *Composite Structures*, Vol. 81, No. 3, 2007, pp. 362–373. doi:10.1016/j.compstruct.2006.08.031

[4] Chaudhuri, R. A., "A New Three-Dimensional Shell Theory in General (Non-Lines-of-Curvature) Coordinates for Analysis of Curved Panels Weakened by Through/Part-Through Holes," *Composite Structures*, Vol. 89, No. 2, 2009, pp. 321–332. doi:10.1016/j.compstruct.2008.07.005

[5] Chaudhuri, R. A., "Three-Dimensional Asymptotic Stress Field in the Vicinity of the Line of Intersection of a Circular Cylindrical Through/ Part-Through Open/Rigidly Plugged Hole and a Plate," *International Journal of Fracture*, Vol. 122, Nos. 1–2, 2003, pp. 65–88. doi:10.1023/B:FRAC.0000005375.68272.c5

[6] Becker, W., "Complex Method for the Elliptic Hole in an Unsymmetric Laminate," *Archive of Applied Mechanics*, Vol. 63, No. 3, 1993, pp. 159–169. doi:10.1007/BF00794890

[7] Persson, E., and Madenci, E., "Composite Laminates with Elliptical Pin-Loaded Holes," *Engineering Fracture Mechanics*, Vol. 61, No. 2, 1998, pp. 279–295. doi:10.1016/S0013-7944(98)00041-1

[8] Chern, S. M., and Tuttle, M. E. "On Displacement Fields in Orthotropic Laminates Containing an Elliptical Hole," *Journal of Applied Mechanics*, Vol. 67, No. 3, 2000, pp. 527–539. doi:10.1115/1.1309545

[9] Chaudhuri, R. A., "An Equilibrium Method for Prediction of Transverse Shear Stresses in a Thick Laminated Plate," *Computers and Structures*, Vol. 23, No. 2, 1986, 139–146. doi:10.1016/00457949(86) 90208-7

[10] Engblom, J. J., and Ochoa, O. O., "Finite Element Formulation Including Interlaminar Stress Calculations," *Computers and Structures*,

Vol. 23, No. 2, 1986, pp. 241–249.
doi:10.1016/0045-7949(86)90216-6

[11] Chaudhuri, R. A., and Seide, P., "An Approximate Method for Prediction of Transverse Shear Stresses in a Laminated Shell," *International Journal of Solids and Structures*, Vol. 23, No. 8, 1987, pp. 1145–1161.
doi:10.1016/0020-7683(87)90052-7

[12] Byun, C., and Kapania,R. K. "Prediction of Interlaminar Stresses in Laminated Plates Using Global Orthogonal Interpolation Polynomials," *AIAA Journal*, Vol. 30, No. 11, 1992, pp. 2740–2749.
doi:10.2514/3.11293

[13] Noor, A. K., Kim, Y. H., and Peters, J. M. "Transverse Shear Stresses and Their Sensitivity Coefficients in Multilayered Composite Panels," *AIAA Journal*, Vol. 32, No. 6, 1994, pp. 1259–1268.
doi:10.2514/3.12128

[14] Rohwer, K., and Rolfes, R., "Calculating 3D Stresses in Layered Composite Plates and Shells," *Mechanics of Composite Materials*, Vol. 34, No. 4, 1998, pp. 355–362.
doi:10.1007/BF02257903

[15] Chaudhuri, R. A., and Seide, P., "An Approximate Semi-analytical Method for Prediction of Interlaminar Shear Stresses in an Arbitrarily Laminated Thick Plate," *Computers and Structures*, Vol. 25, No. 4, 1987, pp. 627–636.
doi:10.1016/0045-7949(87)90270-7

[16] Chaudhuri, R. A., "A Semi-Analytical Approach for Prediction of Interlaminar Shear Stresses in Laminated General Shells," *International Journal of Solids and Structures*, Vol. 26, Nos. 5–6, 1990, pp. 499–510.
doi:10.1016/0020-7683(90)90024-P

[17] Chaudhuri, R. A., Balaraman, K., and Kunukkasseril, V. X., "Admissible Boundary Conditions and Solutions to Internally Pressurized Thin Arbitrarily Laminated Cylindrical Shell Boundary-Value Problems," *Composite Structures*, Vol. 86, No. 4, 2008, pp. 385–400.
doi:10.1016/j.compstruct.2007.12.008

[18] Chaudhuri, R. A., "Computation of Transverse Shear Stresses in the Vicinity of the Circumferential Re-Entrant Corner Line of an Internal Part-Through Hole Weakening an Edge-Loaded Plate," *Composite Structures*, Vol. 89, No. 2, 2009, pp. 315–320.
doi:10.1016/j.compstruct.2008.07.004

[19] Chaudhuri, R. A., "Transverse Shear Stress Distribution through Thickness near an Internal Part-Through Elliptical Hole in a Stretched Plate," *Composite Structures*, Vol. 92, No. 4, 2010, pp. 818–825.
doi:10.1016/j.compstruct.2009.08.019

[20] Chaudhuri, R. A., and Seide, P., "Interlaminar Shear Stresses around an Internal Part-Through Hole in a Laminated Composite Plate," *Composite Structures*, Vol. 92, No. 4, 2010, pp. 835–843.
doi:10.1016/j.compstruct.2009.08.042

[21] Chaudhuri, R. A., and Xie M., "Tale of Two Saints: St. Venant and "St. Nick": Does St. Venant's Principle Apply to Bi-Material Straight Edge and Wedge Singularity Problems?," *Composites Science and Technology*, Vol. 60, Nos. 12–13, 2000, pp. 2503–2515.
doi:10.1016/S0266-3538(00)00044-0

[22] Chaudhuri, R. A., and Chiu, S. J., "Three-Dimensional Asymptotic Stress Field at the Front of an Unsymmetric Bimaterial Wedge Associated with Matrix Cracking or Fiber Break," *Composite Structures*, Vol. 78, No. 2, 2007, pp. 254–263.
doi:10.1016/j.compstruct.2005.09.013

[23] Wang, S. S., and Choi, I., "Boundary-Layer Effects in Composite Laminates: Part 1: Free-Edge Stress Singularities," *Journal of Applied Mechanics*, Vol. 49, No. 3, 1982, pp. 541–548.
doi:10.1115/1.3162514

[24] Chaudhuri, R. A., and Xie, M., "Free-Edge Stress Singularity in a Bimaterial Laminate," *Composite Structures*, Vol. 40, No. 2, 1997, pp. 129–136.
doi:10.1016/S0263-8223(97)00152-9

[25] Chaudhuri, R. A., "An Eigenfunction Expansion Solution for Three-Dimensional Stress Field in the Vicinity of the Circumferential Line of Intersection of a Bimaterial Interface and a Hole," *International Journal of Fracture*, Vol. 129, No. 4, 2004, pp. 361–384.
doi:10.1023/B:FRAC.0000049494.43743.45

[26] Chaudhuri, R. A., and Chiu, S. J., "Three-dimensional Asymptotic Stress Field in the Vicinity of an Adhesively Bonded Scarf Joint Interface," *Composite Structures*, Vol. 89, No. 3, 2009, pp. 475–483.
doi:10.1016/j.compstruct.2008.10.002

[27] Chaudhuri, R. A., and Seide, P., "Triangular Finite Element for Analysis of Thick Laminated Plates," *International Journal for Numerical Methods in Engineering*, Vol. 24, No. 6, 1987, pp. 1203–1224.
doi:10.1002/nme.1620240611

[28] Chaudhuri, R. A., "Analysis of Laminated Shear-Flexible Angle-Ply Plates," *Composite Structures*, Vol. 67, No. 1, 2005, pp. 71–84.
doi:10.1016/j.compstruct.2004.01.002

[29] Seide, P., and Chaudhuri, R. A., "Triangular Finite Element for Analysis of Thick Laminated Shells," *International Journal for Numerical Methods in Engineering*, Vol. 24, No. 8, 1987, pp. 1563–1579.
doi:10.1002/nme.1620240812

[30] Chaudhuri, R. A., and Seide, P., "Triangular Element for Analysis of Perforated Plates under Inplane and Transverse Loads," *Computers and Structures*, Vol. 24, No. 1, 1986, pp. 87–95.
doi:10.1016/0045-7949(86)90337-8

[31] Chaudhuri, R. A., "A Simple and Efficient Plate Bending Element," *Computers and Structures*, Vol. 25, No. 6, 1987, pp. 817–824.
doi:10.1016/0045-7949(87)90197-0

[32] Chaudhuri, R. A., "A Degenerate Triangular Shell Element with Constant Cross-Sectional Warping," *Computers and Structures*, Vol. 28, No. 3, 1988, pp. 315–325.
doi:10.1016/0045-7949(88)90071-5

[33] Arfken, G., *Mathematical Methods for Physicists*, 2nd ed., Academic Press, New York, 1970.

[34] Park, K. C., and Stanley, G. M. "A Curved C^0 Shell Element Based on Assumed Natural-Coordinate Strains," *Journal of Applied Mechanics*, Vol. 53, No. 2, 1986, pp. 278–290.
doi:10.1115/1.3171752

[35] Korn, G. A., and Korn, T. M., Differential Geometry, *Mathematical Handbook for Scientists and Engineers*, 2nd ed., McGraw–Hill, New York, 1968, Ch. 17.

[36] Fung, Y. C., *Foundations of Solid Mechanics*, Prentice-Hall, Englewood Cliffs, NJ, 1965.

M. Hyer
Associate Editor